VOL. 18, NO. 22, NOVEMBER 2023 ISSN 1819-6608
ARPN Journal of Engineering and Applied Sciences

www.arpnjournals.com

DELINEATION OF THE PROPER LOCATIONS FOR WASTEWATER DISPOSAL IN ARID REGIONS USING TEM AND ERT TECHNIQUES: A CASE STUDY AT RUBIKI INDUSTRIAL ZONE, BADR CITY, EGYPT

Usama Massoud[1], Mohamed Attwa[2,3], Abeer El-Kenawy[2] and Mohamed Mosa[2]
[1]National Research Institute of Astronomy and Geophysics, NRIAG, Helwan, Egypt
[2]Zagazig University, Faculty of Science, Zagazig, Egypt
[3]National Authority for Remote Sensing and Space Sciences, Egypt
E-Mail: MIMosa@science.zu.edu.eg

ABSTRACT

Proper wastewater disposal is crucial for the sustainable development of rapidly growing megacities worldwide. The emergence of waterlogging near evaporation ponds (EVP) and in desert areas surrounding these cities poses a significant environmental threat. This study employs an integrated approach, combining transient electromagnetic (TEM) and 2D-electrical resistivity tomography (2D-ERT) methods with remote sensing techniques, to understand wastewater flow patterns around EVPs and identify suitable disposal sites. The research focuses on a complex subsurface structure in the Cairo-Suez district, characterized by extensive surface waterlogging. Initial monitoring relies on satellite imagery and land use-land cover maps. TEM provides an overview of subsurface layer distribution, while 2D-ERT offers detailed insights into near-surface flow paths. To address the limitations of geoelectrical methods in locating conductive layers, advanced inversion techniques (AIS) are applied. The findings reveal a four-layer subsurface composition, with waterlogging primarily attributed to the argillaceous limestone layer interbedded with shale. This layer is shallower in the eastern and northwest areas, correlating with higher instances of waterlogging. Moving northward, the argillaceous limestone layer deepens, and the upper clastic layer thickens, resulting in reduced waterlogging. The study underscores the influence of subsurface structure on near-surface layer distribution. Based on these findings, optimal wastewater disposal sites are recommended, with a focus on the northern region where the argillaceous limestone layer is deeper and the upper clastic layer is thicker. To mitigate waterlogging, the installation of disposal wells is highly advised, leveraging the insights derived from this research. This study offers a versatile and reproducible approach suitable for both pre-project planning and post-project phases in desert regions.

Keywords: waterlogging; desert lands; land-use/land-cover (LU/LC); ERT; TEM.

Manuscript Received 23 September 2023; Revised 12 January 2024; Published 30 January 2024

1. INTRODUCTION

Poorly planned urbanization can have a devastating impact on the environment. Water-logging appearance in new urban areas has become one of the most environmental hazards. This is confirmed by the fact that 80-90% of wastewater produced in underdeveloped nations remains untreated, posing serious hazards to the natural environment (Salem *et al*., 2021). accumulation of wastewater in the shape of waterlogging ponds around industrial areas in desert lands has been linked to aquifer system pollution (Williams *et al*., 2019), in addition to other terrestrial ecosystems (Hejna *et al*., 2020) Additionally, waterlogging can lead to a large surface area of wastewater being exposed to the atmosphere. This can have a negative impact on the climate, as it can release greenhouse gases such as methane and nitrous oxide (Beaulieu *et al.,* 2019). Therefore, it is crucial to assess the suitability of the location where wastewater is disposed of to prevent surface waterlogging and its related impacts.

Recently, the use of the Transient Electromagnetic [TEM] method has become widespread across various domains, including geological structure analysis, geothermal exploration, mapping of Contaminant plumes, and Groundwater investigations(Gómez *et al*., 2019; Gonçalves *et al.,* 2017). This technique has been employed to investigate the lateral and vertical variations in resistivity values for the subsurface layers in the study area. The unique TEM method has proven successful in exploring environmental issues (Gonçalves *et al*., 2017). Several publications (Fitterman and Stewart, 1986; Kanta *et al*., 2013; Nabighian and Macnae, 1991) have detailed the TEM technique. Compared to other geophysical methods, the TEM method excels in determining variations in the uppermost layer and producing high-quality data (Barsukov *et al.,* 2006). The depth of investigation can vary from a few meters to several hundred meters, influenced by factors such as the configuration of the TEM loop, subsurface attributes, and background electromagnetic interference.

The Electrical resistivity tomography [ERT] method has gained significant popularity and has proven effective in resolving various engineering and geo-environmental challenges (Attwa and Henaish, 2018). Moreover, the ERT technique serves as a valuable tool for establishing connections between surface hydrogeological phenomena and subsurface structural (Attwa and Günther, 2012). This is due to the wide range of resistivity values observed in nature and the fact that it represents one of the

simplest and most cost-effective geophysical approaches available. However, it does have limitations, particularly in detecting highly conductive layers. ERT relies on the measurement of electrical resistivity variations in the subsurface. When encountering materials with very high conductivity, such as saline water or clay, the electrical currents tend to flow easily, making it challenging to distinguish and delineate these conductive layers accurately. The method may struggle to provide precise information about the depth, thickness, or geometry of such conductive features, potentially leading to misleading interpretations (Attwa *et al;* 2018). So, an advanced inversion scheme was used to overcome this limitation.

The study area's subsurface characteristics are poorly understood, and the factors influencing surface waterlogging remain unclear. This highlights the significance of the present research, which aims to achieve the following primary objectives: 1) mapping the distribution of near-surface layers that hinder wastewater infiltration and lead to surface waterlogging, 2) evaluating the impact of subsurface structure and topography on waterlogging and wastewater movement, and 3) providing recommendations and potential solutions to mitigate the escalating waterlogging issue in the future.

2. LOCATION OF THE STUDY SITE

The investigated area Rubiki Industrial City is located in the Cairo-Suez district, in the northern part of Badr City, Egypt between Northern latitudes 30°10° and 30°12° and Eastern longitudes 31°42° and 31°50°, as a part of Cairo-Suez district Figure-1a The industrial effluent of all industrial units in Rubiki city is not properly disposed of, with all types of wastewater being discharged into stabilization pond sets. These ponds (lagoons) were built on the city's eastern outskirts. The performance of these ponds is currently diminishing owing to hydraulic overloading and a lack of filtration. Also, due to the limited capacity of these stabilization ponds to absorb increasing amounts of water, wastewater is discharged randomly into the desert. Furthermore, the uncased ponds and drainage network are located on a highly structural site with sandy soil with intercalation of argillaceous materials. As a result, wastewater seepage has been noticed from satellite images and waterlogging has appeared in numerous locations, indicating an environmentally hazardous condition as shown in Figure-1a Moreover, the extent of waterlogging exhibits a substantial increase over time and corresponds to the expansion of urban areas, as proven by the land use-land cover (LU/LC) maps Figure-2 spanning a period of four years, from 2018 to 2022.

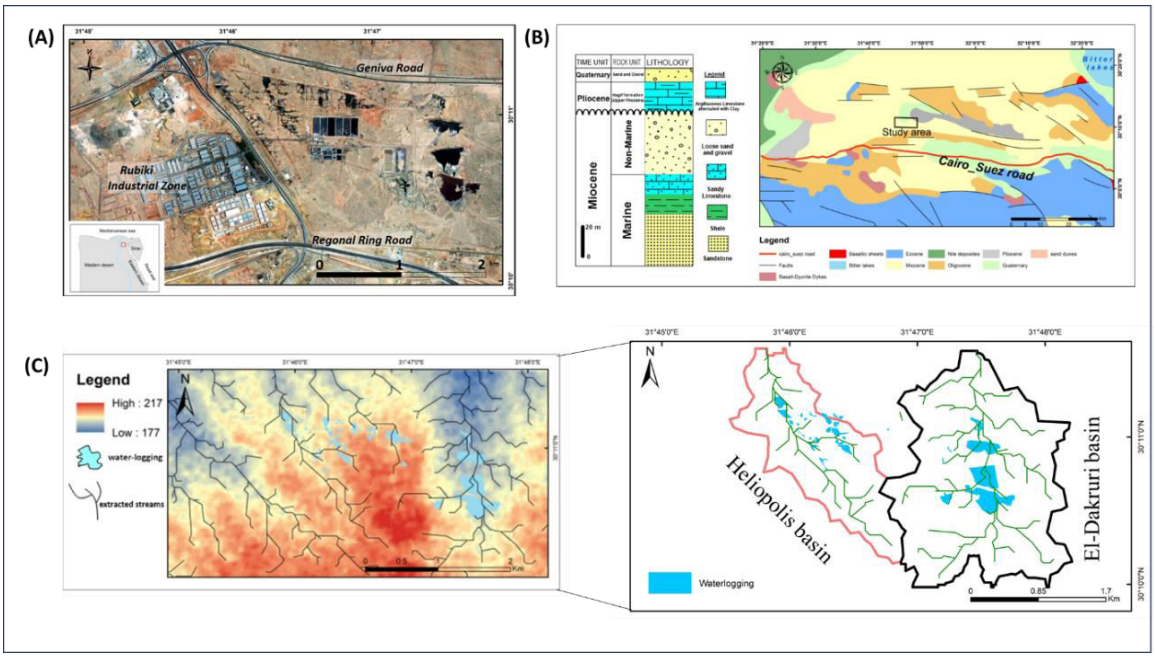

Figure-**1.** [a] Location map of the investigated area. [b] Geological map of Cairo-Suez district shows the orientation of main faults modified after Panagos *et al*., "(2011) and Composite stratigraphic section of the study area modified after Moustafa *et al.,* (1985). [c] Extracted streams over DEM. And main basins in the study site.

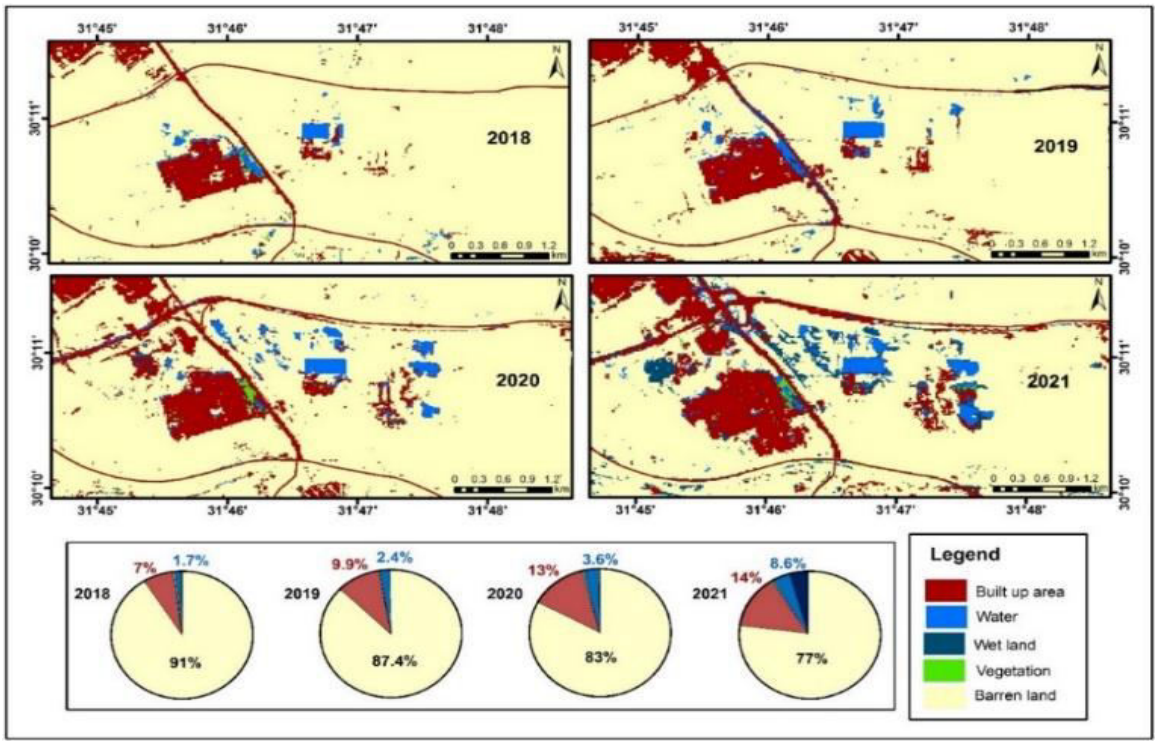

Figure-2. LU/LC of the study site over four years from 2018 to 2021. Shows the multiplication of built-up area percentage from 7% in 2018 to 14% in 2021, and the increase of wetlands and waterlogged percentage from 1.7% in 2018 to 8.6% in 2021.

3. GEOLOGY AND GEOMORPHOLOGY

Our research site is regarded to be a part of the Cairo-Suez district, which is characterized by a complicated tectonic setting. According to Said (1964), the structural framework of the Cairo-Suez area is dominated by two primary sets of faults directed E-W and NW, both of which are of the same age. Also, the stratigraphic column of the study area comprises a sequence of Miocene rocks at the base, followed by Pliocene deposits and overlain by Quaternary clastics Figure-1b. According to (Shukri *et al.,* 1953) the Miocene deposits, which come first at the stratigraphic column in the study site, is divided into two units: marine and non-marine unit. The marine Miocene is made up of sandstone, shale, and sandy limestone, whereas the non-marine unit is made up of unstratified sand and gravel. The eastern part of the study site, as shown in Figure-1b, is dominated by Pliocene deposits, which are represented by Hagif Formation. This formation is formed of shallow marine succession (30 m thick) of thick Limestones alternating with shales and shaly sandstone (Wanas *et al*., 2020). Quaternary clastics come at the top of succession in the form of sand and gravel. From a geomorphological perspective, the region consists of two primary drainage basins Figure-1c terms from east to west: the El-Dakruri basin, which serves as the main watershed towards Cairo-Ismailia Road, and the Heliopolis basin, the main watershed located to the east of Cairo. The Heliopolis basin discharges water to the Damietta branch in the East Nile Delta. Geomorphologically, the digital elevation model (DEM) of the study area, depicted in Figure-1c, illustrates that the ground surface elevation varies from 177 to 217m above sea level (a.s.l). The highest elevations are primarily found in the southern region, while the elevation gradually diminishes towards the northern part. Additionally, based on Figure-1c, it is evident that waterlogging tends to concentrate in areas of lower elevation, following the same direction as the extracted streams. This indicates that waterlogging correlates with the topography and main slope of the area.

4. MATERIALS AND METHODS

4.1 Transient Electromagnetic (TEM) Method

For this research, 36 TEM soundings were conducted using the AIE-2 device, as shown in Figure-3. Data collection involved using a single square loop measuring 50 ^{x} 50 m with an intensity current source ranging between 6 and 8 A, with an average of 7 A for most TEM measurements. The field data were carefully examined, smoothed, edited, or selected based on their significance. The observed data were then transformed from apparent resistivity with time (ρa (t)) to true resistivity with depth (ρ (h)), as depicted in Figure-4. Additionally, six cross-sections (A-A′, B-B′, C-C′, D-D, E-E′, F-F′) were generated from the TEM measurements, as illustrated in Figure-3.

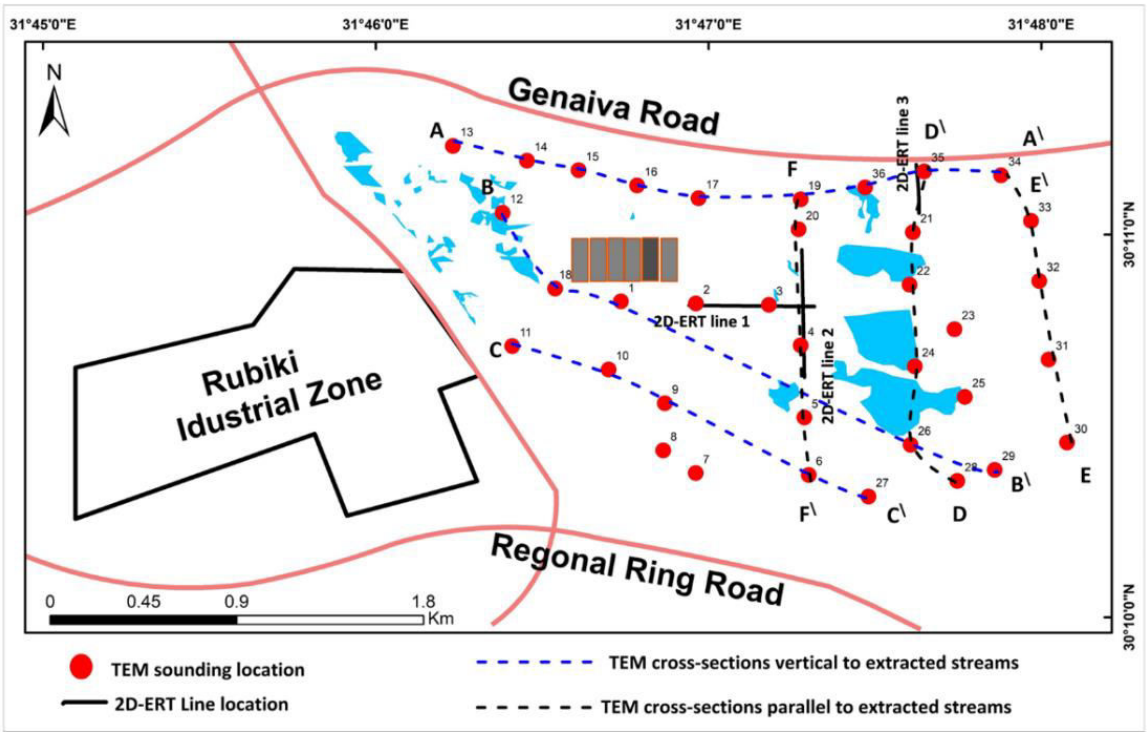

Figure-3. The base map of the study site shows locations of waterlogging (blue color) and geophysical field work.

4.2 2D Electrical Resistivity Tomography (2DERT)

A 2D ERT survey was conducted as a complementary technique to gather more comprehensive subsurface information in both lateral and vertical directions. This method relies on the principles of Direct Current (DC) methods. The apparent resistivity of the subsurface is determined by introducing electrical currents through two electrodes (Current electrodes) and measuring the potential difference between another two electrodes (potential electrodes). To enhance data acquisition, a new automated system with multi-electrodes was utilized (Dahlin, 2001).

For the 2D-ERT lines, the Syscal Pro equipment from IRIS Instruments was employed, using two multicore cables and 48 electrodes. The survey consisted of seven 2D ERT profiles measured in four lines implemented with the Wener array configuration which is known for its robustness, high signal-to-noise ratio, and efficient characterization of horizontal discontinuities (Falae *et al*., 2019). The electrode spacing used was 5 meters. The data levels (n) for each profile were 15. The acquired data number for each 2D-ERT profile was 360. In this work, the 2D-ERT data were processed and interpreted using the DC2DInvRes software package (Günther, 2018). To overcome the constraints of the traditional inversion strategy in the presence of high conductive layers, The Advanced Inversion Scheme (AIS) was employed to invert the (2D-ERT) profiles. This involved integrating prior geological and borehole data into the inversion procedure, where decoupling cells at different depths were introduced within the 2D model. Additionally, the individual model cell boundaries are weighted using a blocky model option (L1 norm inversion). For a detailed AIS explanation, see (Clément *et al.*, 2010). The utilization of AIS has been demonstrated in geo-environmental research within hyper-arid desert terrains (Abotalib *et al.,* 2021; El-Saadawy *et al.,* 2020). This approach effectively mitigated the challenges associated with interpreting geophysical data, leading to a well-justified analysis of data inversion. Consequently, this methodology enabled the generation of dependable inverted models with enhanced resolution.

5. RESULTS AND DISCUSSIONS

5.1 TEM Data Analysis and Interpretation

TEM data field measurements with a loop size of 50*50 m were inverted using the ZONDTEM1D version 5.2 inversion algorithm (Barsukov *et al*., 2006). The maximum estimated depth for these measurements was 120 meters, while the minimum was 50 meters. This depth range is influenced by the presence of a conductive layer, which restricts the current from penetrating deeper subsurface layers. The collected TEM-sounding datasets throughout the study region were mostly characterized by high quality. However, TEM 2 sounding had to be excluded from the analysis due to the presence of recorded noise. For each TEM sounding, an initial model was selected based on the geological information from previous work Fig. (1b) and the lithology available from boreholes and outcrops. The inversion process yielded realistic model fits with RMS errors ranging from 1.5% to 7%. An illustration of the inversion results for TEM 30, along with the lithological descriptions of each layer from the previous geological investigations in the area, can be seen in Figures (4a and b). The inverted TEM measurements revealed four distinct layers in most

locations, while certain TEM soundings showed the presence of three layers instead. The inversion results of 36 TDEM points were integrated in comparison with the available borehole data and the deduced parameters were employed in different locations and directions to form six geo-electrical cross sections; three of them are vertical to streamlines (nearly vertical to waterlogging extension), and the other three cross-sections are parallel to streamlines (same direction as waterlogging extension) (for location, see Figure-3).

The TEM cross-sections (A-A′, B-B′, and C-C′) run vertically to the streamlines, as indicated in Figure-3 by the blue dashed lines. Four main layers are detected; [1] the first orange layer in the cross-sections Figure-5 represents the surface layer, which is a mixture of clay, clayey sand, sand, and gravel. The resistivity of this layer ranges from 20 to 300 ohm.m depending on the percentage of fine materials and the degree of wastewater saturation. [2] The brown layer corresponds to Pliocene Argillaceous Limestone (Argill. L.S) interbedded with shale, exhibiting resistivity values spanning from 3 to 10 ohm.m. This particular layer is accountable for the occurrence of surface waterlogging, primarily because its low permeability hinders wastewater infiltration. [3] The Non-Marine Miocene gravelly sand appears with a pale-yellow color with resistivity ranging from 28 to 80 ohm.m. [4] The Non-Marine Miocene shale layer appears at the base of cross sections with resistivities ranging from 2 to 4 ohm.m. These cross-sections show the large discontinuity of subsurface layers at different locations, which can be referred to as inferred faults, as shown in Figure-5. The increasing accumulation of layer deposits on the downthrown side of these faults is also noticed. Also, by putting these sections in their locations, we can notice that the thickness of layers increases downstream towards the north.

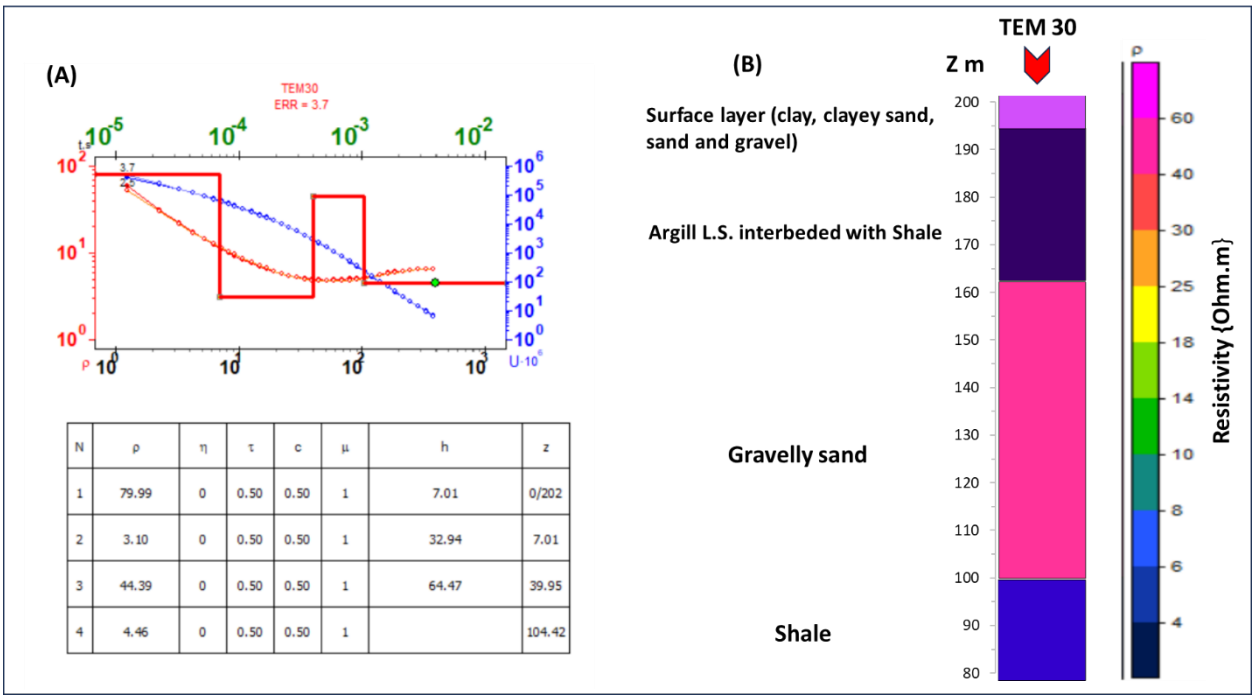

N	ρ	η	τ	c	μ	h	z
1	79.99	0	0.50	0.50	1	7.01	0/202
2	3.10	0	0.50	0.50	1	32.94	7.01
3	44.39	0	0.50	0.50	1	64.47	39.95
4	4.46	0	0.50	0.50	1		104.42

Figure-4. [a] The inversion result of TEM sounding No. 30 using ZONDTEM1D software. Where ρ-the resistivity, η - polarizability ($0 \leq \eta \leq 1$); c - the exponent; τ - relaxation time, h-the thickness (m) and z-depth to layer); [b] lithological description of TEM 30 versus resistivity value for each layer.

On the other hand, Figure-6 shows three cross-sections (D-D′, E-E′, and F-F′) are conducted parallel to the streamlines. From these cross sections Figure-6, we can notice a group of step faults extending in the E-W direction. The downthrown sides of these faults are directed towards the north. So, we can deduce that the basins in the study site are structurally controlled by these step faults.

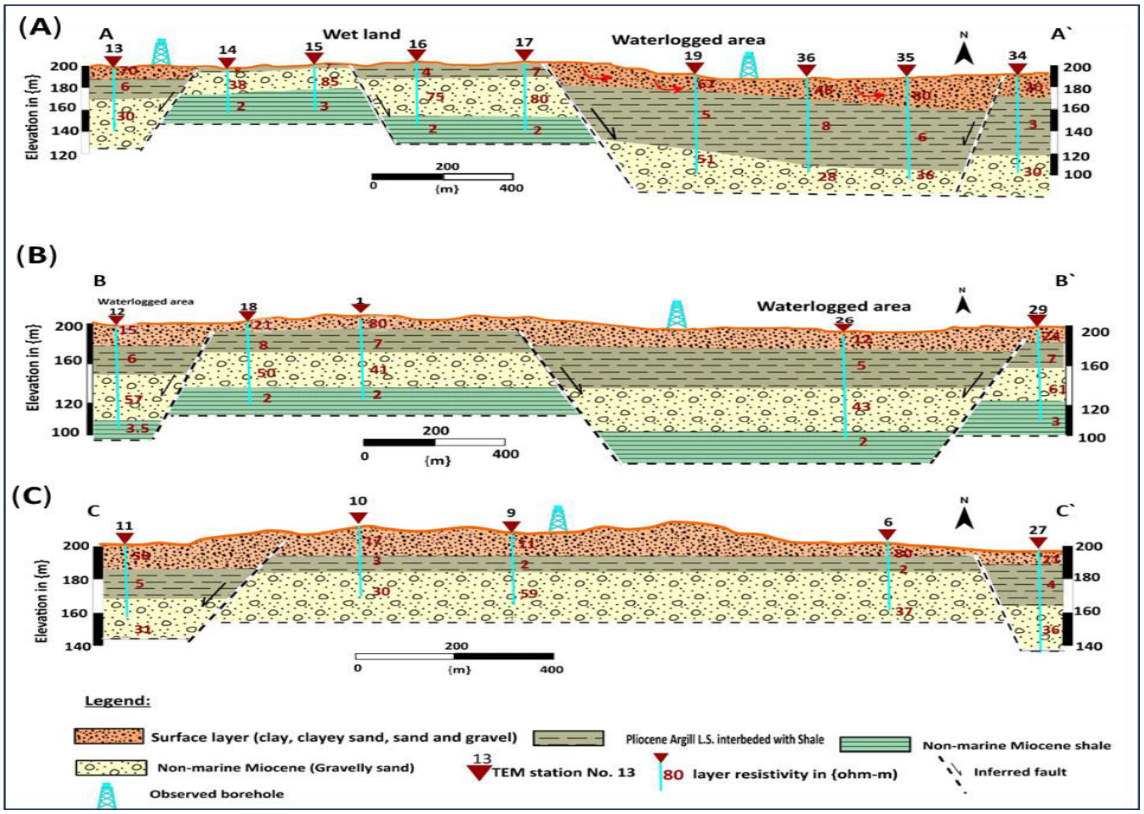

Figure-5. [a] A- A'; [b] B–B′ and [c] C–C′ cross-sections obtained from TEM analysis and vertical to extracted streams.

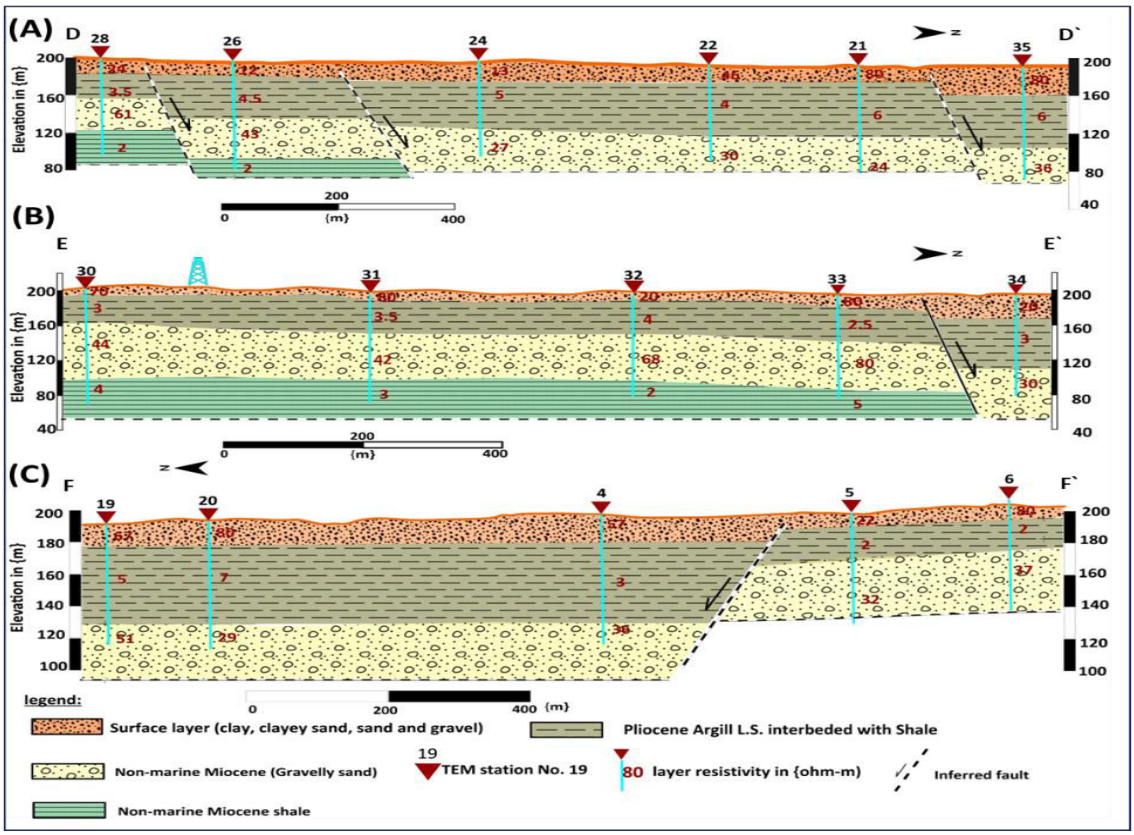

Figure-6. [a] A- A'; [b] B–B′ and [c] C–C′ cross-sections obtained from TEM analysis and parallel to extracted streams.

By examining the six geo-electrical cross-sections, it becomes evident that the depth and thickness of the layers vary across different locations, primarily due to the influence of intense structures such as normal faults. Utilizing the TEM-sounding results, we mapped the depth and thickness of the second layer, which is the Argillaceous Limestone. This layer is of particular significance as it exhibits low permeability, making it a major contributor to surface waterlogging Figure-7. The argillaceous layer is shallower in the east and northwest directions, which is why waterlogging is more common in these areas. The argillaceous layer is also thicker in the east, which contributes to the waterlogging problem. Toward the north, the argillaceous layer becomes deeper and the upper clastic sediments become thicker, which reduces the risk of waterlogging in this area as shown in Figure-7.

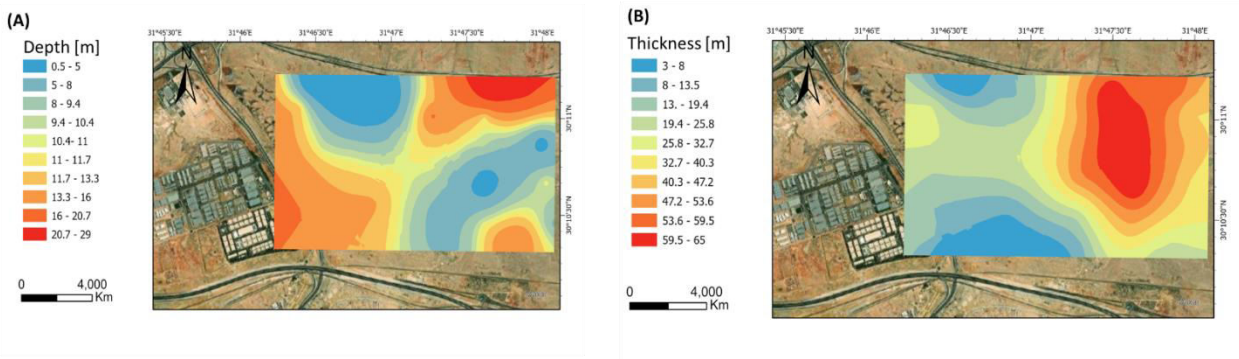

Figure-7. [a] Depth contour map of Argill. L.S layer. [b] Isopach contour map of the Argill. L.S layer.

5.2 ERT Data Inversion and Interpretation

After analyzing the results of the TEM inversion, a 2D Electrical Resistivity Tomography (ERT) survey was carried out to obtain detailed and high-resolution data for shallow depths. The primary aim of this survey was to validate the position and influence of the main structure on the distribution of near-surface layers and to pinpoint the areas most prone to waterlogging problems within the study site.

2D-ERT of line _1

Line_1 was performed in the central part of the investigated area and ran in the West-East direction, crossing TEM1 Figure-3. Line _1 consists of three profiles P1-P2-P3 was measured along one line directed from west to east; after that, the roll-along option was used to merge them into one profile Fig. (8a), 600m long (for location, see Figure-3). The red layer (50:100 ohm.m) of Non-Marine Miocene gravelly sand reaches its maximum thickness (about 30 m) at the western part of the profile Figure-8a. At the eastern part of the profile, there is a noticeable discontinuity in the western layers. This discontinuity can be referred to as a normal fault Figure-8a. At the downthrown side of the fault, the accumulation of Pliocene deposits (intercalation of Argill. L.S. and clayey sand 25:50 ohm.m) increases to reach about 25m thickness, and this explains the appearance of waterlogging in the eastern part of the study site in large quantities as this layer prevents downward infiltration of wastewater due to its low permeability.

2D-ERT of line _2

As 2D-ERT of line _1 was measured to provide insight into the shallow subsurface from west to east, 2D-ERT of line _2 measured vertical to 2D-ERT of line _1 to show subsurface layers distribution from south to north (for locations, see Figure-3). 2D-ERT of line _2 also consists of three profiles P4-p5-p6 which were measured in one line and merged in one profile Fig. (8b) (for location, see Figure-3). The effect of normal fault is very clear Figure-8b. The presence of this fault causes the Pliocene Argill.L.S layer to vanish towards the northern direction. As a result, waterlogging becomes evident in the southern section of the profile due to the heightened content of Pliocene fine materials (clay and Argill.L.S). Conversely, in the northern part, the waterlogging subsides due to the accumulation of coarser materials (sand and gravel).

2DERT of line _3

As mentioned before the waterlogging diminishes in the northern direction, to gain a more distinct understanding of the subsurface in this northward direction line 3 was acquired from south to north (for location, see Figure-3), line _3 comprises a single profile (P7) Figure-8c measured behind the northern waterlogging Pond. Notably, the gravelly sand Layer thickness continues to increase northward as shown in P7 Figure-8c and these deposits enable wastewater to percolate downward due to their high permeability. So, waterlogging disappears towards the north.

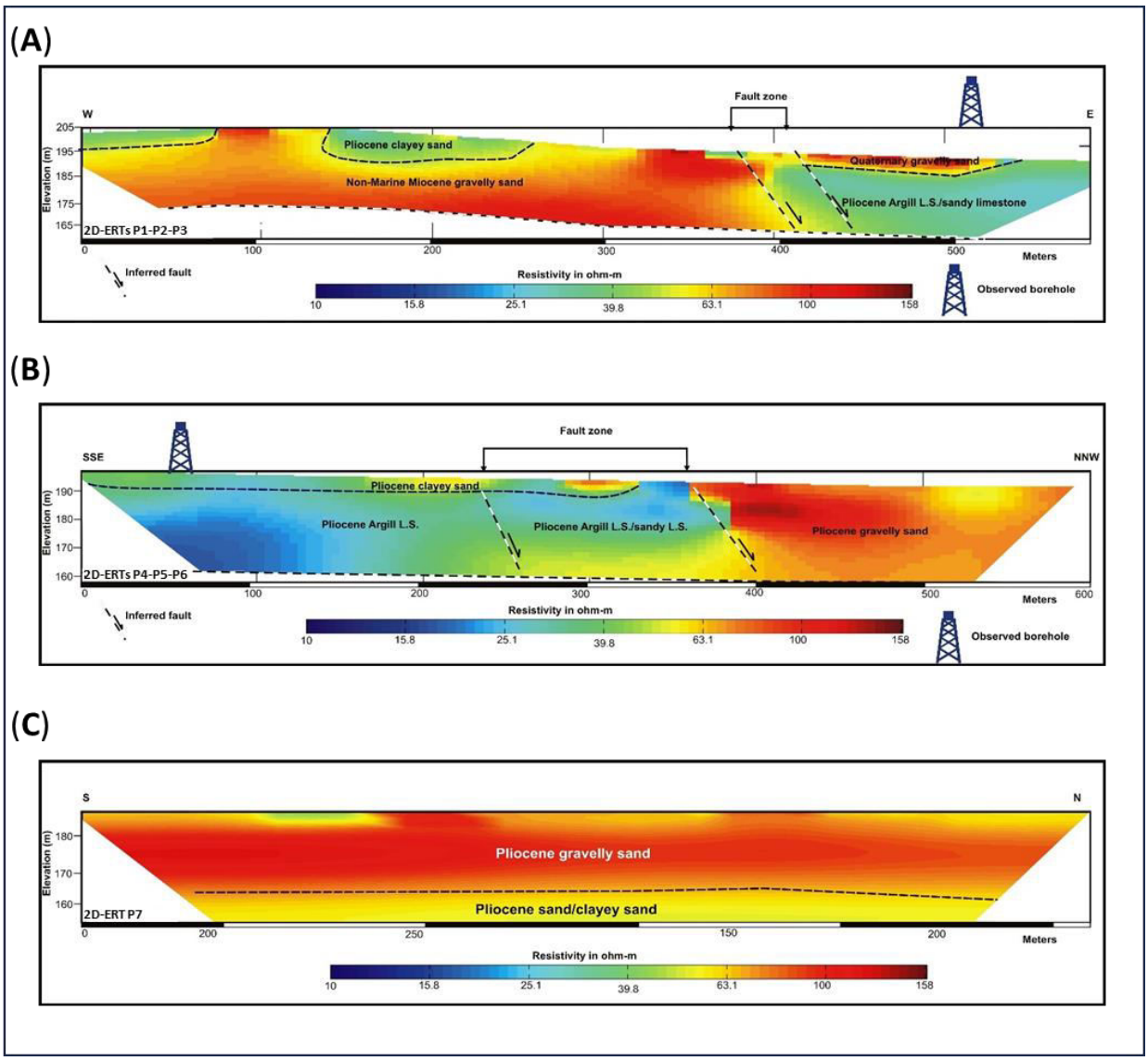

Figure-8. [a], [b] the 2D inverted resistivity imaging model of line 1 and line 2 at the central part of the study area. [c] 2D inverted resistivity imaging model of line 3 at the northern part of the study area. (for their locations, see Figure-3).

4. CONCLUSIONS

This study utilized a combination of TEM and 2D-ERT to delineate the proper locations for industrial wastewater disposal by identifying the factors contributing to surface waterlogging in specific sections of the study site. Through insights gained from geophysical data, we identified an argillaceous layer as the primary reason for waterlogging due to its low permeability. By employing TEM data, we meticulously tracked this layer's characteristics by creating a detailed map of its depth and thickness throughout the study site. The using of AIS in 2D-ERT inversion gives a high-resolution view of near-surface layers and confirms the locations of faults. Our research findings revealed that the argillaceous layer is shallower in the eastern and northwest directions, providing an explanation for surface waterlogging in these areas. Furthermore, this layer's thickness is more prominent in the eastern part of the study site. Moving towards the north, the layer's depth increases, and the thickness of the upper clastic sediments increases, contributing to the reduction of waterlogging towards the northern zone. As the study area is a part of the Cairo-Suez district, the subsurface structure, particularly the presence of normal faults, significantly influences variations in the depth and thickness of subsurface layers and shapes the configuration of all basins within the study area. Ultimately, this research effectively evaluated the study area, identifying potential future waterlogging zones, and offering recommendations to mitigate this environmental concern. So, the research presents a valuable strategy for assessing subsurface conditions, a crucial aspect to consider in the planning of new urban areas to address potential environmental and engineering challenges.

RECOMMENDATIONS

According to our geological and borehole data, the groundwater in the study site is much deeper than the depth we have investigated, so there is no risk of groundwater contamination. We propose two recommendations for wastewater disposal, but further chemical studies on the interaction between wastewater and soil are needed before implementation. The first recommendation is to dispose of excess wastewater in the northern region, where the clastic thickness is greater, which will allow for more efficient absorption of the wastewater. The second recommendation is to use the third layer revealed by TEM cross-sections, which is composed of highly porous sand and gravel sandwiched between two impermeable layers. This porous layer can be used as a disposal storage zone by constructing disposal wells that penetrate the upper impermeable layer and reach the porous layer, ensuring a safe and contained disposal method. From this study, we can choose the most suitable locations for these disposal wells away from faults and fractures and by referring to Figure-7 maps; we can pinpoint areas with shallow depths and a thinner layer of Argill. L.S., which is most appropriate for locating these disposal wells.

ACKNOWLEDGMENT

The authors thank the Center of Excellence for Water in Egypt for providing facilities for field work Additionally, they thank Prof. Said Ragab, Prof. Ayman Ismail, and Prof. Ahmed Henish for their participation.

REFERENCES

Abotalib A. Z., Heggy E., El Bastawesy M., Ismail E., Gad A. and Attwa M. 2021. Groundwater mounding: A diagnostic feature for mapping aquifer connectivity in hyper-arid deserts. Science of the Total Environment, 801, 149760. https://doi.org/10.1016/J.SCITOTENV.2021.149760

Attwa M. and Günther T. 2012. Application of spectral induced polarization (SIP) imaging for characterizing the near-surface geology: An environmental case study at Schillerslage, Germany. Australian Journal of Basic and Applied Sciences, 6(9) 693-701.

Attwa M. and Henai:sh A. 2018. Regional structural mapping using a combined geological and geophysical approach – A preliminary study at Cairo-Suez district, Egypt. Journal of African Earth Sciences, 144, 104–121. https://doi.org/10.1016/J.JAFREARSCI.2018.04.010

Barsukov P. O., Fainberg E. B. and Khabensky E. O. 2006. Chapter 3 Shallow Investigations by TEM-FAST Technique: Methodology and Examples. Methods in Geochemistry and Geophysics, 40(C): 55-77. https://doi.org/10.1016/S0076-6895(06)40003-2

Beaulieu J. J., DelSontro T. and Downing J. A. 2019. Eutrophication will increase methane emissions from lakes and impoundments during the 21st century. Nature Communications, 10(1). https://doi.org/10.1038/S41467-019-09100-5

Clément R., Descloitres M., Günther T., Oxarango L., Morra C., Laurent J. P. and Gourc J. P. 2010. Improvement of electrical resistivity tomography for leachate injection monitoring. Waste Management, 30(3): 452-464. https://doi.org/10.1016/J.WASMAN.2009.10.002

Dahlin T. 2001. The development of DC resistivity imaging techniques. Computers and Geosciences, 27(9): 1019-1029. https://doi.org/10.1016/S0098-3004(00)00160-6

El-Saadawy O., Gaber A., Othman A., Abotalib A. Z., Bastawesy M. El and Attwa M. 2020. Modeling Flash Floods and Induced Recharge into Alluvial Aquifers Using Multi-Temporal Remote Sensing and Electrical Resistivity Imaging. Sustainability, 12: 10204, 12(23): 10204. https://doi.org/10.3390/SU122310204

Falae P. O., Dash R. K. and Kanungo D. P. 2019. Geo-electrical characterization of Tangni landslide, Garhwal Himalayas, India. 1st Indian Near Surface Geophysics Conference and Exhibition, 273-280. https://doi.org/10.3997/2214-4609.201979046

Fitterman D. V. and Stewart M. T. 1986. Transient electromagnetic sounding for groundwater. Geophysics, 51(4): 995-1005. https://doi.org/10.1190/1.1442158

Gómez E., Larsson M., Dahlin T., Barmen G. and Rosberg J. E. 2019. Alluvial aquifer thickness and bedrock structure delineation by electromagnetic methods in the highlands of Bolivia. Environmental Earth Sciences, 78(3): 1-13. https://doi.org/10.1007/S12665-019-8074-X/FIGURES/10

Gonçalves R., Farzamian M., Monteiro Santos F. A., Represas P., Mota Gomes A., Lobo de Pina A. F. and Almeida E. P. 2017. Application of Time-Domain Electromagnetic Method in Investigating Saltwater Intrusion of Santiago Island (Cape Verde). Pure and Applied Geophysics, 174(11): 4171-4182. https://doi.org/10.1007/S00024-017-1642-7/FIGURES/8

Günther T. 2018. Software DC2DINVRES. Direct current 2D inversion and resolution.

Hejna M., Moscatelli A., Stroppa N., Onelli E., Pilu S., Bald A. and Rossi L. 2020. Bioaccumulation of heavy metals from wastewater through a Typha latifolia and Thelypteris palustris phytoremediation system. Chemosphere, 241. https://doi.org/10.1016/j.chemosphere.2019.125018

Kanta A., Soupios P., Barsukov P., Kouli M. and Vallianatos F. 2013. Aquifer characterization using

shallow geophysics in the Keritis Basin of Western Crete, Greece. Environmental Earth Sciences, 70(5): 2153-2165. https://doi.org/10.1007/S12665-013-2503-Z/FIGURES/6

Moustafa A. R., El-Nahhas F. and Abdel Tawab S. 1985. Structural Setting of the Area East of Cairo, Maadi, and Helwan. Middle East Research Center, Ain Shams University Scientific Research Series., 5, 40-64.

Nabighian M. N. and Macnae J. C. 1991. 6. Time Domain Electromagnetic Prospecting Methods. Electromagnetic Methods in Applied Geophysics, 427-520. https://doi.org/10.1190/1.9781560802686.CH6

Panagos P., Jones A., Bosco C. and Senthil Kumar P. S. 2011. European digital archive on soil maps (EuDASM): Preserving important soil data for public free access. International Journal of Digital Earth, 4(5): 434-443. https://doi.org/10.1080/17538947.2011.596580

Said R. 1964. Review of the Geology of Egypt: by Rushdi Said. In American Journal of Science. 262: 1237-1238).

Salem H., Gemail K., Hydrology A. N.-J. C. and 2021, undefined. (n.d.). A multidisciplinary approach for delineating wastewater flow paths in shallow groundwater aquifers: A case study in the southeastern part of the Nile Delta, Egypt. Elsevier. Retrieved October 27, 2022, from https://www.sciencedirect.com/science/article/pii/S016977 2220302904

Shukri N. M, AKMAL M. G. 1953. The geology of gebel EL Nasuri and Gebel EL Anqabiya district.

Wanas H. A., Khalifa M. M. and Mousa F. A. 2020. A contribution to the lithostratigraphy of the Plio-Pleistocene succession in the area southwest of Wadi El-Natrun , north Western Desert, Egypt A contribution to the lithostratigraphy of the Plio-Pleistocene succession in the area southwest of Wadi El-N. January, 0-28.

Williams M., Kookana R. S., Mehta A., Yadav S. K., Tailor B. L. and Maheshwari B. 2019. Emerging contaminants in a river receiving untreated wastewater from an Indian urban centre. Science of the Total Environment, 647, 1256-1265. https://doi.org/10.1016/j.scitotenv.2018.08.084